Probabilistic Model for 3D Discrete Cracking Concrete in Parallel Computing

Camen N. Mena Paz[1], Luiz F. Martha[1], Eduardo, M.R. Fairbairn[2], José L.D. Alves[2], Nelson F.F. Ebecken[2] and Alvaro L.G.A. Coutinho[2]

[1]Department of Civil Engineering
Pontifical Catholic University of Rio de Janeiro, (PUC-Rio)
Street Marquês de São Vicente 225, 22453-900 - Brazil
{mena,lfm}@tecgraf.puc-rio.br

[2]COPPE/UFRJ - Program of Civil Engineering
PO Box 68506, 21945-970
Federal University of Rio de Janeiro - Brazil
eduardo@labest.coc.ufrj.br, jalves@lamce.ufrj.br , nelson@ntt.ufrj.br , alvaro@nacad.ufrj.br

Abstract. This work presents a probabilistic crack approach (Rossi and Ulm, [1], [2], [3], [4]), based on the Monte Carlo method, that was recently implemented in a 3D fully parallelized finite element code Paz, [5]. The cracking scheme used is the discrete crack approach introduced by 3D interface elements. In this approach the heterogeneity of the material is taken into account by considering the properties to vary spatially following a normal distribution firs statical distribution is then determined by the mean the standard deviation of the considered material properties. If the heterogeneous characteristics of the material are well established and quantified by the statistical moments it is possible that the model displays the size effects related to the material heterogeneity.
Fracturing is modeled by 3D interface elements generated in a previously defined region within the mesh. The interface elements are triangular base prisms connecting adjacent faces of neighboring tetrahedra. These elements simulate crack opening through relative displacements between the triangular faces (Paz [5]).
The implemented code developed for a shared memory, parallel vector processor (PVP) environment, more to be execurate and efficient to run Monte Carlo simulations of a strongly non linear problem.

1 Introduction

Among several other relevant factors, such as water/cement ratio of the paste, casting and curing conditions, loading conditions, etc, concrete cracking depends on the random distribution of constituents and initial defects. The heterogeneity governs the overall cracking behavior and related size effects on concrete fracture. The probabilistic crack approach, based on the direct Monte Carlo method, developed by Rossi and co-workers (Rossi *et al.* [1], [2], [3], [4]) takes this stochastic process into account by assigning in finite element analysis, randomly distributed material properties (tensile strength, Young's modulus) to both the solid elements and the contact elements interfacing the former (discrete crack approach). The stochastic process is introduced at the local scale of the material, by considering that cracks are created within the concrete with different energy

dissipation depending on the spatial distribution of constituents and initial defects. The local material behavior in concrete is assumed to obey a perfect elastic brittle behavior, so that the random distribution of local cracking energies can be replaced by a random distribution of local strengths. Therefore, solid elements are elastic, while interface elements are considered brittle elastic (almost rigid brittle).

The present probabilistic model involves a number of mechanic properties of the material to be determined, which constitutes the modeling data. From a large number of direct tensile tests, it was found that a normal law describes rather well the experimental distribution (Rossi *et al.* [2]). These characteristics are: $f_{ct,\mu}$ and E_μ, the means of the tensile strength and of the Young's modulus respectively; $f_{ct,\sigma}$ and E_σ, the standard deviations of the tensile strength and of the Young's modulus, respectively. The following analytical expressions were proposed:

$$f_{ct,\mu} = 6.5\,(V_t / V_g)^{-a}; \qquad f_{ct,\sigma} / f_{ct,\alpha\mu} = 0.35\,(V_t / V_g)^{-b} \tag{1}$$

$$E_\mu = E \qquad E_\sigma / E = 0.15\,(V_t / V_g)^{-c} \tag{2}$$

where: V_t is the volume of the two finite elements contiguous to an individual contact element of the mesh; V_g is the volume of the coarsest aggregate; E is the average Young's modulus which does not exhibit significant volume effects. For cylinder specimens, whose dimensions are 160 mm in diameter and 320 mm high a,b,c are constants related to it's compressive strength f_c given by:

$$\begin{aligned} a &= 0.25 - 3{,}6\times10^{-3}(f_c) + 1.3\times10^{-5}(f_c)^2 \\ b &= 4.5\times10^{-2} + 4.5\times10^{-3}(f_c) - 1.8\times10^{-5}(f_c)^2 \\ c &= 0.116 + 2.7\times10^{-3}(f_c) - 3.4\times10^{-6}(f_c)^2 \end{aligned} \tag{3}$$

In these expressions, the compressive strength f_c represents the quality of the concrete matrix, while the volume of the coarsest aggregate V_g, refers to the elementary material heterogeneity.

Equations (1) to (3) show that the smaller the scale of observation, the larger the fluctuation of the local mechanical properties, and thus the (modeled) heterogeneity of the matter. In other words, the finer the mesh, the greater the modeled heterogeneity in terms of Young's modulus and tensile strength. The empirical expressions corresponding to equations (1) to (3) were calibrated to fit a number of material tests for different types of concretes and volumes. They give a first approximation to capture volume effects on concrete fracture; but they are not expected to be universal. Furthermore, little is known about the validity of these empirical formulas for small V_t / V_g these volume ratios which maybe used in finite element structural analysis, are too little to be determined by means experimental tests.

The mesh has m_v volume elements and m_i interface elements. Each interface element follows an a elastic-brittle constitutive law characterized by an individual tensile strength $\mathbf{f}_{ct,ii}$ and individual Young's modulus, of the volume elements is referenced by $\mathbf{E}_{iv}$.

Following Rossi et al. [2] findings these individual local tensile strengths and Young's modulus are represented by normal distributions having the densities:

$$g_f(f_{ct}) = \frac{1}{f_{ct,\sigma}\sqrt{2\pi}} \exp\left[-\frac{1}{2}\left(\frac{f_{ct,\mu}}{f_{ct,\sigma}} \right)^2 \right] \tag{4}$$

$$g_E(E) = \frac{1}{E_\sigma \sqrt{2\pi}} \exp\left[-\frac{1}{2}\left(\frac{E - E_\mu}{E_\sigma} \right)^2 \right] \tag{5}$$

with: $g_f(f_{ct})$ and $g_E(E)$ the density function for the tensile strength f_{ct} and the Young's modulus E, respectively; while x_μ and x_σ denote the mean and standard derivation of the distribution of quantity x. For the problem at hand, it is possible to find a sample of m_i values $\mathbf{f}_{ct,ii}$, each value corresponding to an interface element and m_v values $\mathbf{E}_{iv}$ each value corresponding to a volume element by using a standard routine for generation of random numbers for a given normal distribution (Press *et al*., [6]).

If the heterogeneous characteristics of the material are well established and quantified by the statistical moments it is possible that the model displays the size effects related to the material heterogeneity. The problem with this approach is that these statistical moments are not known, a priori, for the characteristic volume of the finite elements used in analysis. However, some methods have been proposed to determine these parameters by means of inverse analysis using neural networks (Fairbairn *et al*, [7],[8]).

The solution for this probabilistic approach is obtained by means of a Monte Carlo simulation. A number of n samples is generated (for a given normal distribution) and some characteristic responses of the structure (for example, stress crack-width $\sigma - w$ curve, or load displacement $P - \delta$ curve) are computed. Let the *j*th samples correspond to, e.g., the *j*th $\sigma - w$ curve. This *j*th $\sigma - w$ curve is composed of discrete values, σ_k^j and w_k^j, where the superscript j indicates the sample and the subscript k the discrete value of the $\sigma - w$ curve. The same discrete $w-$ values are assumed and the response is defined exclusivily by the values of σ_k^j . The mean curve composed by pairs σ_k^{mean}, w_k then simply reads

$$\sigma_k^{mean,j} = \frac{1}{j}\sum_{l=1}^{j} \sigma_k^l \tag{6}$$

The Monte Carlo simulation is stopped when

$$\left| \sigma_k^{mean,j} - \sigma_k^{mean,j-1} \right| \le tol \tag{7}$$

where *tol* is the prescribed tolerance to check the convergence of the procedure. With the convergence of the procedure, the total number of samples is set to $n = j$. This total number of samples *n*, corresponding to a Monte Carlo converged simulation, clearly depends on *tol*, which is a measure of the precision required by the analysis. It also depends on the heterogeneity of the material represented by the standard deriation. The more heterogeneous is the material the greater is the number of samples necessary to obtain a converged solution. Our experience in this field indicates that 25 to 50 samples are sufficient to obtain a converged $\sigma - w$ curve.

2. Discrete cracking: The interface elements

The finite element cracking model is a discrete model for which volume elements are always elastic and cracking occurs in elastic-brittle (almost rigid brittle) contact elements placed between two volume elements. The interface elements 3D (Paz, [5]) depicted in Fig. 1 can be thought as triangular base prisms connecting adjacent faces of neighboring tetrahedra.
These elements are formulated to describe relative displacements between the triangular faces to simulate crack opening.

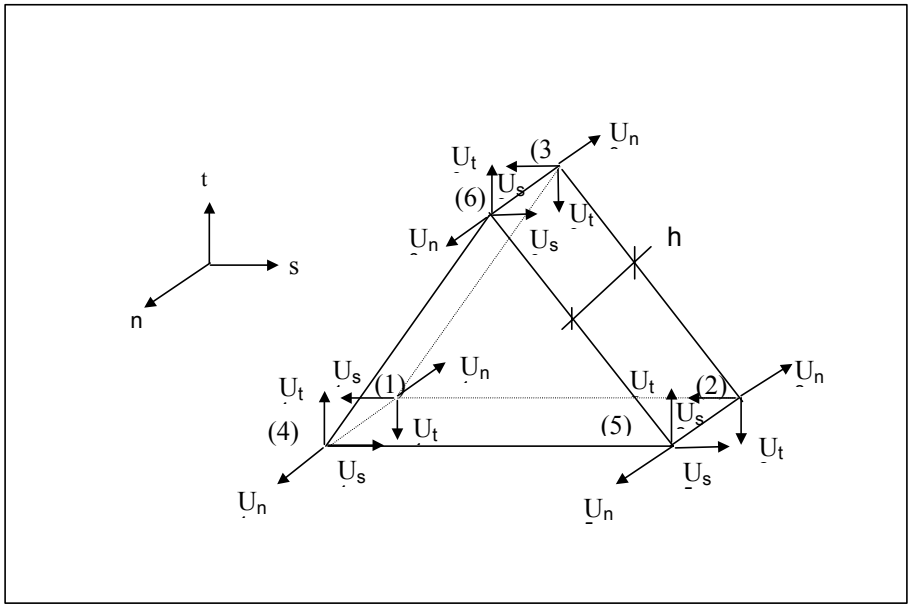

Fig. 1. An Interface Element and its degrees of freedom in a local system

The constitutive law of the 3D interface element is defined by equation (8) for non cracked elastic state characterized by $\sigma_n < f_{ct,i}$. When the tensile strength is reached the elements attains the cracked stage and module E_c and G_c are set to zero (figure 2).

$$\Delta\boldsymbol{\sigma} = \mathbf{D}_{cr}\ \Delta\mathbf{w} = \begin{Bmatrix} \Delta\sigma_n \\ \Delta\sigma_s \\ \Delta\sigma_t \end{Bmatrix} = \begin{bmatrix} E_{c/h} & 0 & 0 \\ 0 & G_c/h & 0 \\ 0 & 0 & G_c/h \end{bmatrix} \begin{Bmatrix} \Delta w_n \\ \Delta w_s \\ \Delta w_t \end{Bmatrix} \tag{8}$$

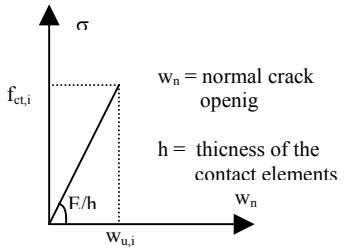

Fig. 2. Elastic-Brittle Contact law

In equation (8) the subscripts *n, s* and *t* indicate the directions normal and transversal to the crack plane respectively, *w* are the relative displacements between the two faces of the interface element, *h* is the width of interface element, E_c and G_c are the longitudinal (Young's) and the transversal modulus respectively.
Equations (8) and figure 2 define the elasto-fragile constituve behavior. However it can be considered rigid-fragile, since thickness *h* of the interface element is considered very small (less than a value $h_{\lim}$) of such form that the solution of the problem does not get excited if *h* diminishes, $h < h_{\lim}$. In this way the modulus E_c and G_c in equation (8) does not have a physical meaning and the terms E_c / h and G_c / h tend to infinity.
The kinematic relation for the interface element is given by:

$$\Delta \mathbf{w} = \mathbf{B}\, \Delta \mathbf{a}_l^e \tag{9}$$

with

$$\mathbf{B} = \frac{1}{3}\begin{bmatrix} -1 & 0 & 0 & -1 & 0 & 0 & -1 & 0 & 0 & 1 & 0 & 0 & 1 & 0 & 0 & 1 & 0 & 0 \\ 0 & -1 & 0 & 0 & -1 & 0 & 0 & -1 & 0 & 0 & 1 & 0 & 0 & 1 & 0 & 0 & 1 & 0 \\ 0 & 0 & -1 & 0 & 0 & -1 & 0 & 0 & -1 & 0 & 0 & 1 & 0 & 0 & 1 & 0 & 0 & 1 \end{bmatrix} \tag{10}$$

$$\mathbf{a}_l^e = \left\{ \mathrm{u}_\mathrm{n}^1\ \mathrm{u}_\mathrm{s}^1\ \mathrm{u}_\mathrm{t}^1 \quad \mathrm{u}_\mathrm{n}^2\ \mathrm{u}_\mathrm{s}^2\ \mathrm{u}_\mathrm{t}^2 \quad \mathrm{u}_\mathrm{n}^3\ \mathrm{u}_\mathrm{s}^3\ \mathrm{u}_\mathrm{t}^3 \quad \mathrm{u}_\mathrm{n}^4\ \mathrm{u}_\mathrm{s}^4\ \mathrm{u}_\mathrm{t}^4 \quad \mathrm{u}_\mathrm{n}^5\ \mathrm{u}_\mathrm{s}^5\ \mathrm{u}_\mathrm{t}^5 \quad \mathrm{u}_\mathrm{n}^6\ \mathrm{u}_\mathrm{s}^6\ \mathrm{u}_\mathrm{t}^6 \right\}^\mathrm{T} \tag{11}$$

The stiffness matrix interface for the element is given by:

$$\mathbf{K}_{\mathrm{Intf}}^{\mathrm{e}} = \int_{\Omega} \mathbf{B}^T\, \mathbf{D}_{cr} \mathbf{B}\, \mathrm{d}\Omega \tag{12}$$

The stiffness coefficients have the same dimension of the stiffness coefficients of the tetrahedra elements (dimension 1/L). This can be verified because matrix **B** is adimensional and $\mathbf{D}_{cr}$ has dimension of $1/(\mathrm{L}^2\ \mathrm{L})$. The resultiling dimension of $\mathbf{K}^e$ is then: $1\frac{1}{L^2 L}1L^2 = \frac{1}{L}$.
The interface elements are automatically generated contiguous to the faces of selected tetrahedra elements. This selection is performed by the user defining a 3D box inside the mesh that contains the target elements.
As it has been described in section 1, within a Monte Carlo simulation the 3D FE solution of the non-linear problem is called for a large member of times. Hence the computer code should be optimized and the flowing section will detail the implementation strategies.

3. Implementation code strategies, parallel vector processor (PVP)

3.1. Solution of equilibrium equations and the inexact Newton Method

Traditional finite element technology for nonlinear problems involves the repeated solution of systems of sparse linear equations by a direct solution method, that is, some variant of Gauss elimination. The updating and factorization of the sparse global stiffness matrix can result in extremely large storage requirements and a very large number of floating point operations.

In this paper we employ an Inexact Newton method (Kelley, [9]), to solve large-scale three dimensional incremental elastic-brittle problems. In the Inexact Newton Method, at each nonlinear iteration, a linear system of finite element equations is approximately solved by the preconditioned conjugate gradient method.
In the finite element method, the implementation of global matrix-vector products are easily parallelized in different computer architectures, performing element level products followed by global assembly. This type of implementation is often referred to element-by-element (EBE) schemes. Matrix-vector products computed by EBE schemes are memory intensive, requiring more operations than the product with the assembled matrix, because element matrices have many overlapping non-zero entries. However, particularly for largescale nonlinear problems EBE methods have been very successful, because they handle large sparse matrices in a simple and straightforward manner. Besides, efficient preconditioners may be derived keeping the same data structure. For a recent review of such topics see Ferencz and Hughes [10].
When solving iteratively the finite element system of linear equations, it is straightforward to employ inexact versions of the standard Newton-like methods (Kelley, [9], Papadrakakis, [11]). In this case, tolerances for the inner iterative driver may be adaptively selected to minimize computational effort towards the solution, giving rise to the following algorithm:

Given u_{tol}, r_{tol}, η relative and residual tolerance.

Compute stiffness tetrahedra matrix $\mathbf{K}_{Tetra}$

do k=1,2….., number of load increments do

Compute external forces vector

$$\mathbf{F}_{ext}^{k} = \mathbf{F}_{nodal}^{K} + \mathbf{F}_{volume} + \mathbf{F}_{\bar{\sigma}} - \left(\mathbf{K}_{tetra}\, \bar{\mathbf{U}}_k + \mathbf{K}_{Intef}\, \bar{\mathbf{U}}_k \right)$$

do i=1,2 ..., while convergence

Compute internal forces vector,

$$\mathbf{F}_{\text{int}}^{i} = \left(\mathbf{F}_{\text{int}}^{i} \right)_{Tetra} + \left(\mathbf{F}_{\text{int}}^{i} \right)_{Intf}$$

Compute residual vector,

$$\boldsymbol{\psi}^{i} = \mathbf{F}_{\text{int}}^{i} - \mathbf{F}_{ext}^{i}$$

Update stiffness interface matrix $\mathbf{K}_{\text{Intf}}^{\text{i}}$

Assembly matrix

$$\mathbf{A}^{i} = \mathbf{K}_{Tetra} + \mathbf{K}_{Intf}^{i}$$

Compute tolerance for iterative driver , η_i

Solver: $\mathbf{A}^{i}\ \Delta\mathbf{u} = \boldsymbol{\psi}^{i}$ for tolerance η_i

Update solution,

$$\mathbf{U} = \mathbf{U} + \Delta\mathbf{u}$$

if $\dfrac{\| \Delta\mathbf{u} \|}{\| \mathbf{U} \|} \le utol$ and $\dfrac{\| \Delta\boldsymbol{\psi}^{i} \|}{\| \mathbf{F}_{ext}^{k} \|} \le rtol$ then convergence

end while i.

end do k.

Note that in $\mathbf{F}_{ext}^{k}$ we account for nodal forces, body forces and prescribed displacements and stresses $\bar{\mathbf{U}}, \bar{\boldsymbol{\sigma}}$. The total internal forces vector $\mathbf{F}_{\text{int}}^{i}$ is the sum of the tetrahedra element vector internal forces $\left(\mathbf{F}_{\text{int}}^{i}\right)_{Tetra}$ plus the interface element internal forces vector $\left(\mathbf{F}_{\text{int}}^{i}\right)_{Intf}$. The total stiffness matrix is the sum of the continuum matrix $\mathbf{K}_{Tetra}$ plus the inteface matrix $\mathbf{K}_{Intf}^{i}$ update at every nonlinear iteration.

We adopted a simple nodal block-diagonal preconditioner. Therefore, the most expensive computational kernel in the linear solver is the matrix-vector product.

According to the above algorithm, an approximate solution is obtained when the Inexact Newton termination criterion is satisfied, that is, when,

$$\left\| \mathbf{A}^{i}\, \Delta\mathbf{u} - \boldsymbol{\psi}^{i} \right\| \leq \eta_i \left\| \boldsymbol{\psi}^{i} \right\| \tag{13}$$

The tolerance η_i may be selected using the expression (Papadrakakis, [11]). We selected η_i as suggested by Kelley [9], based on a measure of how far the nonlinear iteration is from the solution, that is,

$$\eta_i^A = \min\left(\eta_{\max}, \gamma \frac{\left\| \boldsymbol{\psi}^{i} \right\|^2}{\left\| \boldsymbol{\psi}^{o} \right\|^2} \right), \qquad 0 < \gamma < 1 \tag{14}$$

If η_i^A is uniformly limited away from 1, and taking $\eta_i = \max\left(\eta_{\min}, \eta_i^A\right)$ Kelley [9] has shown general convergence properties when Eq. (14) is used. To avoid that η_i^A be too small when the nonlinear iteration is away from the solution, Kelley also suggests the following modification,

$$\eta_i^B = \begin{cases} \min\left(\eta_{\max}, \eta_i^A\right) & ,if\ \gamma\, \eta_{i-1}^2 < 0.1 \\ \min\left(\eta_{\max}, \max\left(\eta_i^A, \gamma\, \eta_{i-1}^2\right)\right) & ,if\ \gamma\, \eta_{i-1}^2 \geq 0.1 \end{cases} \tag{15}$$

In some cases $\|\boldsymbol{\psi}_i\|$ can be very small, well beyond the required accuracy, resulting in undesired work. To remedy this oversolving Kelley [6] proposes to compute η_i^C using;

$$\eta_i^C \left(\eta_{\max}, \max\left(\eta_i^B, 05\ rtol \frac{\left\| \mathbf{F}_{ext}^{k} \right\|}{\left\| \boldsymbol{\psi}^{i} \right\|} \right) \right) \tag{16}$$

and finally taking $\eta_i = \max\left(\eta_{\min}, \eta_i^C\right)$.

Our experience indicates that selecting $\eta_{\max}, = 0.1$ *and* $10^{-3} \leq \eta_{\min} \leq 10^{-6}$ for *utol* and *rtol* in the usual range, that is, 10^{-3} to 10^{-2}, is enough for practical engineering computations. Typical values for γ and *g* are 0.5 and 0.1, respectively.

3.2 Matrix-vector products element-by-element, EBE - general aspects the computing parallel

In the element-by-element EBE matrix-vector product, the matrix $\mathbf{A}$ it is never formed, being the product gives as:

$$\mathbf{A}\,\mathbf{p} = \sum_{e=1}^{Nel} \mathbf{A}_e\mathbf{p} = \sum_{i=1}^{N_{tetra}} \left(\mathbf{K}_{Tetra} \quad \mathbf{p}_i \right) + \sum_{i=1}^{N_{Intf}} \left(\mathbf{K}_{Intf} \quad \mathbf{p}_i \right) \tag{17}$$

where *Nel* is the number of elements in the mesh, N_{tetra} is the number of tetrahedral, N_{intf} is the number of interface elements, $\mathbf{A}_e$ are the element matrices for the tetrahedra and interface; $\mathbf{p}_e$ the components of $\mathbf{p}$ restricted to the degrees of freedom of the element. The arrays of the element stiffness matrices are stored taking into account their symmetry; in the case of the element tetrahedra 78 coefficients are stored and for the interface element only 18 coefficients are stored, exploring the particular structure of the discrete gradient operator given in equation (10).
Note that, during the nonlinear iterations, only the interface element stiffness matrices should be updated.
The mesh coloring algorithm Hughes [10] was extended in order to block both solid and interface into disjoint groups this enabling full vectorization an parallelism of the operations involved in equation (17).

4. Numerical simulation and comparison with experimental data

The experimental results of concrete uniaxial tension tests published by (Li *et al* [12]) were used to ilustrate the developments presented in this paper. The specimens are cylinders 101.6 mm in diameter and 203.2 mm high. This specimens had 25.4 mm notches at their midheight on both sides (Figure. 3).
Concrete with maximum aggregate diameter of 9.525 mm was used. Its average tensile strength and Young's modulus at the age of 28 days were: $f_{ct} = 4{,}72 \quad MPa$ and $E_c = 42000 \quad MPa$.

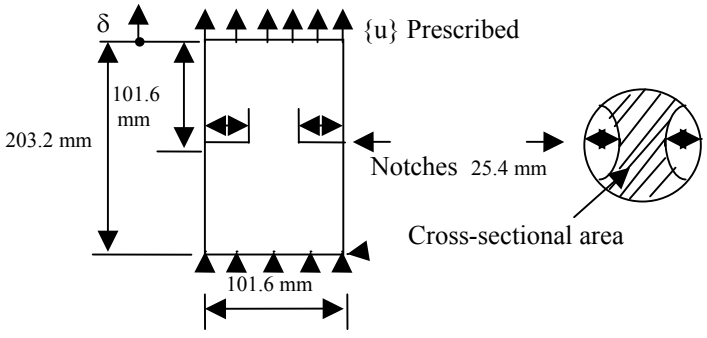

Fig. 3. Uniaxial tension specimen geometry , dimensions, load , boundary conditions and place of the measurement of δ

The numeric experiments were controlled by a field of uniform displacements applied at the upper end of the test specimen. The boundary conditions restrain the degrees of freedom in the vertical at the lower end and place of the measurement of δ (Figure. 3). The mesh of tetrahedra is shown in Figure. 4.

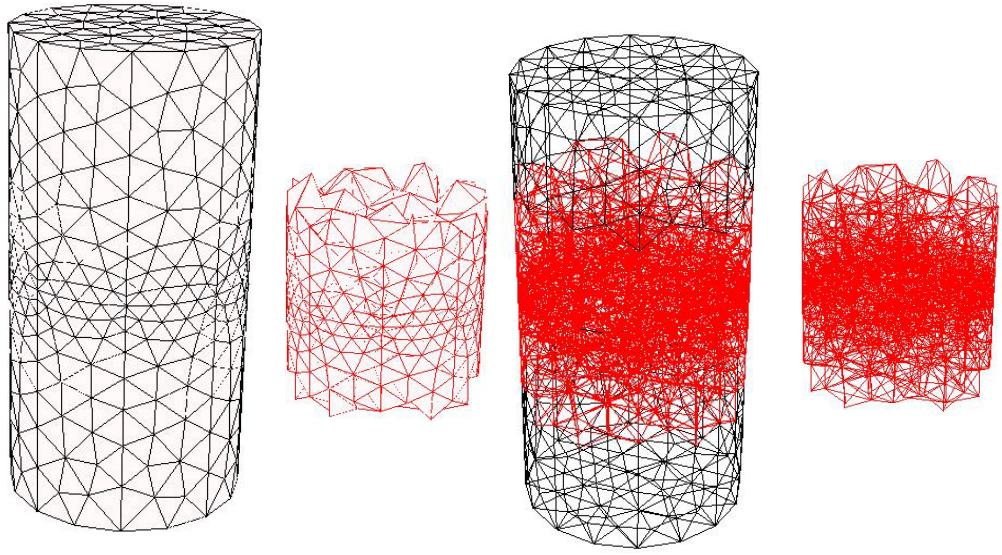

Fig. 4. Mesh of finite elements tetrahedra with inteface elements and detail of the mesh of interface elements

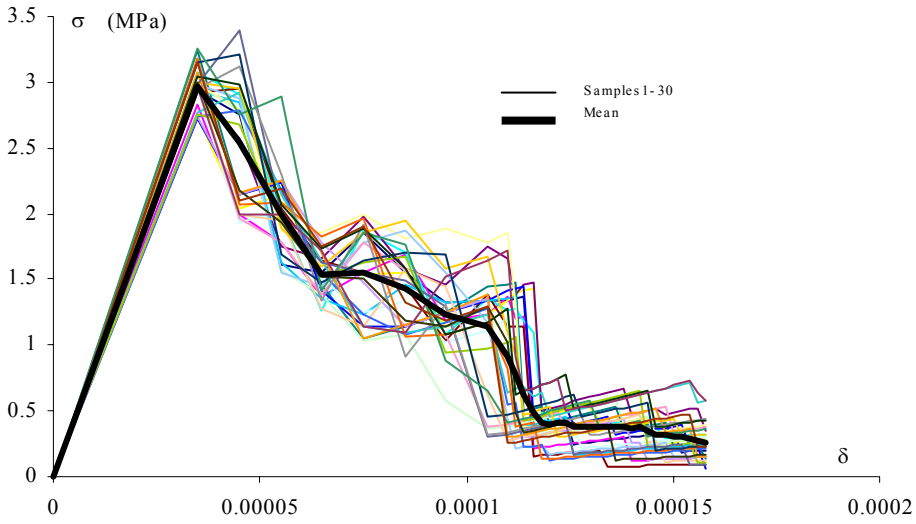

Fig. 5. Monte Carlo simulation

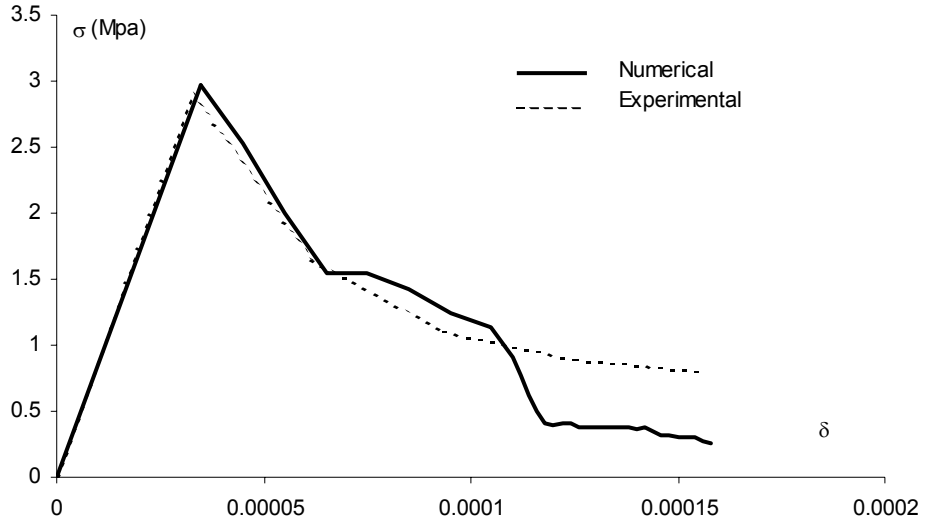

Fig.6. Comparation of experimental and numerical results.

Curves $\sigma - \delta$ for the several samples of the Monte-Carlo simulation are given in figure 5. (place of the measurement of δ (Figure. 3)).The comparison between experimental by Li *et al* [12] and the converget Monte Carlo $\sigma - \delta$ curve is given in figure 6. With the experienc gotten in the works [5], [7], [8] and [14], we are using inverse analisis to introduce factor 2 that it multiplies $f_{ct,\mu}$ of eq. (1).

Figure 7 presents the crack configuration for a given sample at a stage corresponding to the softening branch of the $\sigma - \delta$ curve

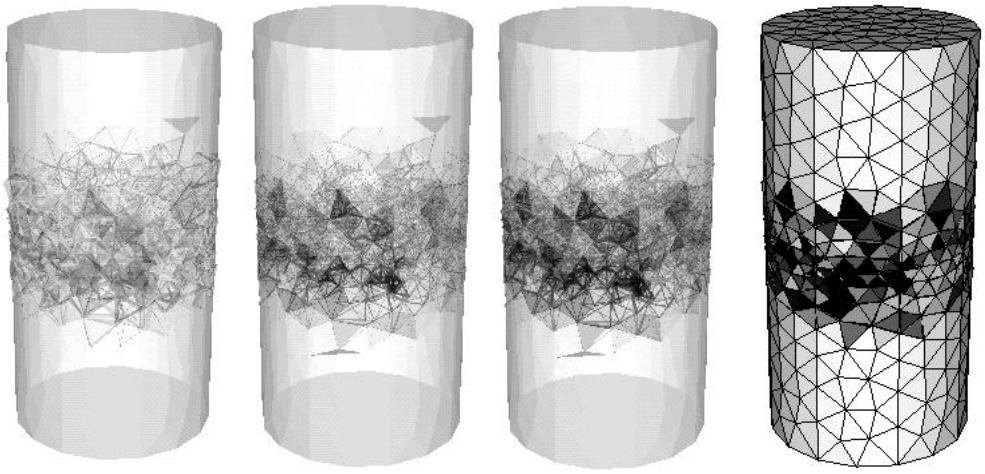

Fig. 7. Crack evolution for numerical simulation

4 Computational aspects of code

4. 1 Convergence Rate

Diagonal and block diagonal preconditioner were compared and results are shown in table 1 for two meshes of the addressed problem

PCG	N^0 steps	N^0 element	N^0 elements tetrahe-dra	N^0 elements interface	N^0 iterations preconditioner diagonal	N^0 iterations preconditioner Block-diagonal	% acelera-tion of con-vergenge for precondi-tioner
Newton Method Tol 10^{-2}	30	856	360	496	1.551.001	1535.939	10
Newton Method Tol 10^{-2}	30	11.933	4.775	7.158	33.985.754	33.654.766	10

Table 1. Acceleration of the convergence using block diagonal preconditionater.

In table 2 we present the results for the two implementations of the inexact Newton Method i.e. Papadrakakis, [11]). And Kelley [9].

PCG – Inexact Newton Method Tol[10^{-6}1, 10^{-1}]	N^0 steps	N^0 element	N^0 elements tetrahe-dra	N^0 elements interface	N^0 iterations precondi-tioner diagonal	N^0 iterations precondi-tioner Block-diagonal	% aceleration of convergenge for preconditioner and Inexact Newton Method
Kelley	30	856	360	496	714.567	707.294	54
Papadrakakis					702.418	695.453	55
Kelley	30	11.933	4.775	7.158	17.141.400	16.991.688	50
Papadrakakis					17.158.720	16.988.676	50

Table 2 . Acceleration of the convergence using Inexact Newton Method

4.2 Computational Performance

A detailed vector performance analysis is obtained by the program summary of the PERFVIEW's Report showed in table 3. The CPU time of the vectorized single processor run for CRAY T90 is 34.87 hours. This table relates the single CPU utilization to the Mflop/s rates for the three top routines. The routines **Smatv-fint** and **Smatv-tetra** are respectively responsible for, the matrix-vector operations on the interface elements and tetrahedra elements, these multiplications are needed in the routine called **PCG-block,** which is the iterative solver to the nodal block di-agonal preconditioner Conjugate Gradient Method.

Routines	Single CPU (%)	Performance (Mflop/s)
smatv-intf	52.80	613.7
smatv-tetra	17.32	554.0
PCG-block	25.90	82.4
Others	3.98	-

Table 3 Performance Analysis -The top 3 subroutines

The code achieved good vectorization on the CRAY T90 for a mesh with 11933 elements, which 7158 are interface and 4775 are tetrahedra elements. The top three subroutines consume the major CPU utilization in the whole analysis. The difference between **smatv-intf** and **smatv-tetra,** in terms of CPU utilization, is coherent with the amount of elements numbers treated by them.
The parallel performance is shown in table 4 and the figures 8 (a) and (b) give a summary report about the ATEXPERT, autotasking performance tool. The top five subroutines stated for parallel analysis are presented in table 4. The routines **Fint-tetra** and **Fint-intf** evaluate respectively the internal force vector of the interface elements and the tetrahedra elements. The interface blockage stiffness matrix, is scattered by **A-Kintf**.

Routines	% Parallel	Dedicated Speedup	Actual Speedup
Smatv-tetra	98.9	3.96	3.8
Smatv-intf	99.8	3.83	3.8
Fint-tetra	92.5	3.83	3.2
Fint-intf	99.1	3.55	3.5
A-Kintf	85.8	3.53	2.6

Table 4 Summary of the ATEXPERT's Report for the 5 dominant loops

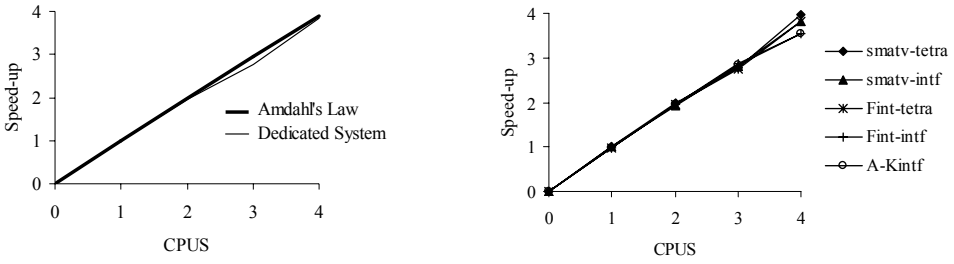

(a) (b)

Fig.8 (a) Program Summary of the ATEXPERT's Report
(b) ATEXPERT's Report -The top 6 subroutines on a Dedicated Speedup

According to ATEXPERT tool this program appears to be 99.2 percent parallel and 0.8 percent serial. Amdahl's Law predicts the program could expect to achieve a 3.9 times speedup on 4 cpus. A 3.8 speedup is predicted with 4 cpus on a dedicated system.

5. Concluding remarks

This paper presented the optimized implementation of Rossi's a probabilistic model for the simulation of cracking in concrete structures. This model in based on the presumption that some particularities of the cracking behavior of concrete, such as strain softening, cracking evolutionand size-effects are derived from the heterogeneous characteristics of the material.

The statistical distribution is determined for a reference discretized material volume (i.e., the FE-volume of two tetrahedra elements interfaced by a contact element). This allows for the determination of probabilistic strength domain of concrete from structural test results, and this for material volumes (equal to the discretization volume), which are normally not accessible to experimental observation (i.e., direct tensile test). The example presented in this paper shown that the model is capable to simulate either the crack opening and the crack pattern.

The probabilistic methodology presented in this paper corresponds to the 3D analysis of a strongly nonlinear material that develops cracking. Besides this fact, the finite elements analysis is called several times within a Monte Carlo simulation.

Therefore, the code should be optimized in such a way that performing such simulations becomes practible

The code achieved a very good level for both parallel performance and vetorization. The most demanding routines, which implement the matrix-vector-multiply computational kernel for the interface and tetrahedral elements, are "fully" parallel (~ 99%) and responsible for over 80% of CPU time. The results emphasizes the suitability of the implemented code on the parallel-vector machine, CRAY T90 for 2 CPU's, which presented a flop rate of 614 Mflop/s and a parallel real speed-up of 3.8 for 4 CPU's.

Extensive use of element-by-element techniques within the computational kernels comprised in the iterative solution drivers provided a natural way for achieving high flop rates and good parallel speed-up's. Besides, by using element-by-element techniques, we avoided completely the formation and handling of large sparse matrices. Therefore, the computational strategies presented herein provide a natural way o deal with more complex scenarios, particularly those involving three-dimensional problems.

Acknowledgments

The authors are indebted to the Computer Graphics Technology Group TECGRAF/PUC-Rio, High Performance Computing Center NACAD/COPPE/UFRJ, and the Laboratory of Computational Methods in Engineering of the Program of Civil Engineering LAMCE /COPPE/UFRJ. CESUP/UFRGS is gratefully acknowledged for the computer time provided for the performance experiments.

This work was partially supported by CAPES and CNPq's grant N^{o} 150039/01-8(NV).

References

1. Rossi P., Richer S.: Numerical modeling of concrete cracking based on a stochastic approach. Materials and Structures, 20 (119), . (1987) 334-337.
2. Rossi P., Wu X., Maou F. le, and Belloc A.: Scale effect on concrete in tension. Materials and Structures, 27 (172), (1994) 437-444.
3. Rossi P., Ulm F.-J., and Hachi F.: Compressive behavior of concrete: physical mechanisms and modeling. Journal of Engineering Mechanics ASCE, 122 (11), (1996), 1038-1043.
4. Rossi P. and Ulm F.-J.: Size effects in the biaxial behavior of concrete: physical mechanisms and modeling. Materials and Structures, 30 (198), (1997) 210-216.

5. Paz C. N. M., Development and Implementation Probabilistic Model for 2D and 3D Discrete Cracking Concrete in Parallel Computing, D.Sc. Thesis, COPPE/UFRJ, the Graduate Institute of Federal University of Rio de Janeiro, Brazil (2000) [in Portuguese].

6. Press W. Teukolski H., S., Vetterling W.T. and Flannery B.: Numerical Recipes, Cambridge University Press (1992).

7. Fairbairn E. M. R., Paz C. N. M., Ebecken N. F. F., and Ulm F-J., Use of neural network for fitting of probabilistic scaling model parameter, Int. J. Fracture, 95, (1999), 315-324.

8. Fairbairn E. M. R., Ebecken N. F. F., Paz C. N. M., and Ulm F-J.: Determination of probabilistic parameters of concrete: solving the inverse problem by using artificial neural networks, Computers and Structures, 78, (2000) 497-503.

9. Kelley C. T.: Iterative Methods for Linear and Nonlinear Equations. Frontiers in applied mathematics, SIAM Society for Industrial and Applied Mathematics, Philadelphia, (1995).

10. Hughes T. J. R., Ferenez R. M. , Hallquist J. O.: Large-Scale Vectorized Implicit Calculation in Solid Mechanics on a CRAY X-MP/48 Utilizing EBE Preconditionated Conjugate Gradients Computer Methods in applied Mechanics and Engineering, 61, (1987) 2115-248.

11. Papadrakakis M.: Solving Large-Scale Problems in Mechanics: The Development and Application of Computational Solution, Editor, M. Papadrakakis, John Wiley and Sons, (1993).

12. Li Q. and Ansari F.: High Concrete in Uniaxial Tension, ACI Material J. 97- (1), (2000) 49- 57.

13. Coutinho A. L. G. A., Martins M. A. D., Alves J. L. D., Landau L., and Moraes A. : Edge-based finite element techniques for nonlinear solid mechanics problems , Int. J. for Numerical Methods in Engineering, 50 (9), (2001) 2050-2068.

14. Fairbairn E. M. R., Debeux V.J.C., Paz C. N. M., and Ebecken N. F. F.: Application of probabilistic Approach to the Analysis of gravity Dam Centrifuge Test, 8^{th} ASCE Specialty Conference on Probabilistic Mechanics and Structural Reliability (2000) PMC 2000-261.

15. Kelley C. T.: Iterative methods for optimization. Frontiers in applied mathematics, SIAM Society for Industrial and Applied Mathematics, Philadelphia, (1999).